Optics Letters

Azimuthal-rotation evanescent-wave illumination incoherent scattering microscopy (AR-EISM) for label-free, high-contrast imaging

Songlin Yang,[1,*] Dingcheng Qi,[1] Qingan Tang,[1] Ran Ye,[1,2] and Yong-Hong Ye[1]

[1] School of Computer and Electronic Information, Nanjing Normal University, Nanjing 210023, China
[2] ran.ye@njnu.edu.cn
*slyang@njnu.edu.cn

Received 17 August 2026; revised 27 September 2026; accepted 2 October 2026; posted 2 October 2026; published 22 October 2026

Evanescent-wave (EW) illumination provides high sensitivity and high signal-to-noise ratio (SNR) for label-free imaging. However, coherent illumination introduces speckle and interference artifacts, while single-direction illumination leads to direction-dependent spatial resolution. Here, we propose azimuthal-rotation evanescent-wave illumination incoherent scattering microscopy (AR-EISM), which continuously rotates incoherent illumination over 360° during a single exposure to reduce the directional dependence of spatial resolution. Imaging experiments with polystyrene nanoparticles using EW illumination with a transverse wavevector of approximately $1.3k_0$ demonstrate that AR-EISM achieves a lateral resolution close to the theoretical Abbe diffraction limit, together with a 1.37-fold increase in SNR and higher imaging contrast compared with conventional dark-field microscopy. These findings highlight the potential of AR-EISM for high-contrast, label-free imaging.
© 2026 Optica Publishing Group. All rights, including for text and data mining (TDM), Artificial Intelligence (AI) training, and similar technologies, are reserved.

https://doi.org/10.1364/OL.614608

Label-free optical imaging is essential for investigating biological structures and nanomaterials without introducing exogenous labels. However, the weak scattering of many nanoscale and biological specimens makes high-resolution, high-contrast imaging challenging. Various label-free imaging techniques have been developed to address this limitation. Dark-field microscopy (DFM) suppresses direct illumination and selectively collects sample-scattered light, enhancing contrast against a dark background [1]. Differential interference contrast (DIC) microscopy converts optical path-length gradients into intensity variations through polarization-based interference [2], whereas quantitative phase imaging (QPI) retrieves sample-induced phase information as measurable intensity contrast [3]. Interferometric scattering microscopy (iSCAT) enhances the detection of weak scatterers through interference between the sample-scattered and reference fields, enabling highly sensitive detection of individual nanoparticles [4,5].

Evanescent-wave (EW) illumination enables high-contrast, surface-selective imaging by confining excitation to the vicinity of an interface through total internal reflection (TIR). Its shallow penetration depth suppresses background signals from deeper regions while enhancing light–matter interactions near the interface, supporting applications in fluorescence imaging and single-molecule detection [6–8]. Incoherent illumination based on evanescent waves or photoluminescence suppresses coherent interference and speckle noise, enabling stable, high-contrast label-free imaging [9–11]. Incoherent averaging of coherent scattering images acquired under EW illumination from different azimuthal directions can further enhance resolution beyond the diffraction limit [12]. Rotating coherent scattering (ROCS) microscopy achieves high-contrast, label-free super-resolution imaging by scanning a coherent laser beam over a 360° azimuthal range during a single exposure [13]. An improved TIR-ROCS system, combining faster beam scanning with optimized illumination, achieved 160 nm spatial resolution at 100 Hz for imaging rapid cellular dynamics [14]. Evanescent-wave-induced spatial-frequency shifting (SFS) can shift otherwise inaccessible high-spatial-frequency information into the far-field detection range, enabling super-resolution imaging [11,15].

Although EW-based label-free super-resolution imaging has been demonstrated through SFS and ROCS, incoherent EW imaging remains attractive because of its simpler, more cost-effective implementation and its ability to suppress speckle and coherent-interference artifacts. Here, we propose azimuthal-rotation evanescent-wave illumination incoherent scattering microscopy (AR-EISM), which employs a hemispherical lens for TIR illumination and rotates incoherent incident light over a full 360° azimuthal range during a single exposure. By integrating images acquired from multiple azimuthal orientations, AR-EISM reduces the directional dependence of spatial resolution and provides improved SNR and imaging contrast compared with conventional DFM. Compared with TIR-ROCS, AR-EISM achieves near-diffraction-limited lateral resolution without requiring specialized TIR objectives and galvanometric scanning, providing a simpler and more cost-effective solution when super-resolution is not required.

The system was based on a standard reflection microscope (Olympus BXFM) with minor modifications (Fig. 1). An LED source with a center wavelength of 510 nm was used for illumination. The emitted beam was first collimated by an

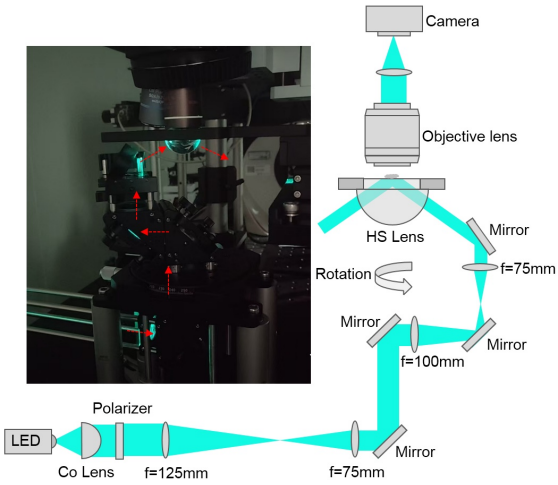


Fig. 1. Schematic of the AR-EISM. Co Lens, collimating lens; HS Lens, hemispherical lens.

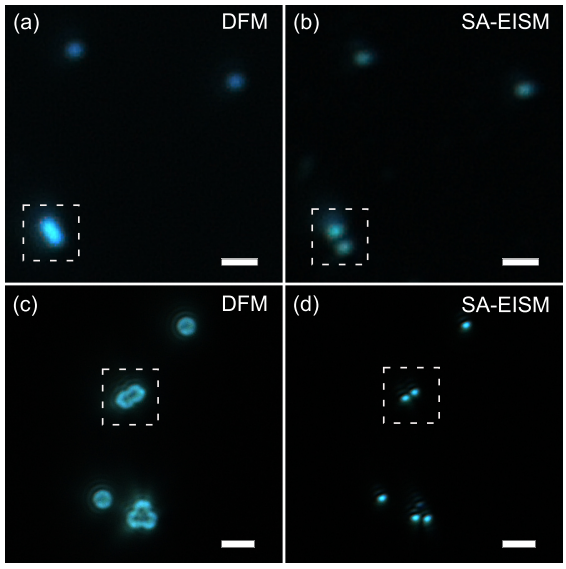


Fig. 2. Imaging of PS particles. (a), (c) DFM images; (b), (d) SA-EISM images. The particle diameters in (a), (b) and (c), (d) are 150 nm and 710 nm, respectively. Exposure time: 1 s. Scale bars: 1 μm.

aspheric condenser lens and then successively reduced in diameter through two beam-reduction stages. Mirrors subsequently redirected the beam onto a BK7 glass hemispherical lens ($n = 1.51$) at an incidence angle of 60°. TIR occurs at the upper surface of the BK7 glass slide ($n = 1.51$), generating an evanescent field with a transverse wavevector of approximately $1.3k_0$ for sample illumination. The lower surface of the slide was optically coupled to the hemispherical lens using an index-matching liquid ($n = 1.51$). The second-stage beam-reduction assembly was mounted on a rotational stage, enabling continuous rotation of the illumination beam about the center of the hemispherical lens and adjustment of the azimuthal angle of the evanescent-wave illumination. The rotational stage was driven by a stepper motor and completed one full 360° rotation within 1 s, synchronized with the camera exposure time. Thus, the camera continuously integrated the scattering signal over the full azimuthal rotation during a single exposure. Light scattered by the sample was collected by a 100× objective lens (Olympus MPlanFL N 100×/0.90 BD P) and imaged onto a color camera (Zeiss AxioCam MRc5) through a tube lens. Intensity profiles were extracted from the blue channel of the 48-bit RGB images using ImageJ. The mean and standard deviation of pixel intensities within selected regions of interest were obtained using the *Analyze* > *Measure* function in ImageJ.

To evaluate single-azimuth evanescent-wave illumination incoherent scattering microscopy (SA-EISM), we compared its performance with conventional DFM. As shown in Fig. 2, the 150-nm PS particles indicated by the boxes cannot be resolved by DFM but appear as two distinct scattering spots under SA-EISM, indicating improved lateral resolution. For the 710-nm particles, DFM resolves the particle edges, although the scattering spots partially overlap (Fig. 2(c)). In contrast, SA-EISM clearly separates the two particles, although their complete contours remain unresolved (Fig. 2(d)).

In AR-EISM, the incoherent illumination was continuously rotated over a 360° azimuthal range during a single exposure, with scattering signals from multiple azimuthal directions integrated to reduce the directional dependence of spatial resolution. Figures 3(a)–3(c) show images of 150-nm-diameter PS particles acquired by DFM, SA-EISM, and AR-EISM, respectively. The signal-to-noise ratio (SNR) was calculated as $(I_{particle} - I_{bg})/\sigma_{bg}$, where $I_{particle}$ is the mean intensity within a 4 × 4-pixel region centered on a particle, and I_{bg} and σ_{bg} are the mean intensity and standard deviation, respectively, within a 200 × 200-pixel particle-free background region. Based on the mean measurements obtained from 30 PS particles and 10 particle-free regions, $I_{particle}$, I_{bg}, and σ_{bg} were 30055, 2653, and 250 for DFM, and 28954, 930, and 186 for AR-EISM, respectively. These values yielded SNRs of 110 and 151, respectively, corresponding to a 1.37-fold increase in SNR with AR-EISM. In addition, the Fourier spectra of the SA-EISM and AR-EISM images span a broader spatial-frequency range than the spectrum of the DFM image. The SA-EISM spectrum exhibits slight elongation along the EW propagation direction, indicating directional modulation of the spatial-frequency distribution induced by EW illumination.

Representative images of closely spaced PS particles with different center-to-center separations are shown in Fig. 3. The valley-to-peak ratio (VPR) is defined as $(I_{valley} - I_{bg})/(I_{peak} - I_{bg})$, where I_{peak}, I_{valley}, and I_{bg} are the peak, valley, and mean background intensities, respectively. For DFM, the VPR at a center-to-center separation of 360 nm was 0.813, exceeding the Rayleigh criterion of 0.735 and indicating that the two particles were unresolved. At a separation of 540 nm, the particles were clearly resolved. For SA-EISM, particles at all three separations were resolved when the illumination direction was parallel to the line connecting their centers, whereas only the particle pair with a center-to-center separation of 540 nm was resolved when the illumination direction was perpendicular to this line. For AR-EISM, a VPR of 0.751 was obtained at a center-to-center separation of 290 nm, which was close to the Rayleigh criterion, indicating that the two particles were marginally resolved. The particles were clearly resolved at center-to-center separations of 360 nm and 540 nm. The imaging contrast was further quantified as $[(I_{peak} - I_{bg}) - (I_{valley} - I_{bg})]/[(I_{peak} - I_{bg}) + (I_{valley} - I_{bg})]$. For DFM, the imaging contrasts at the three separations were 0, 0.113, and 0.391, respectively, whereas

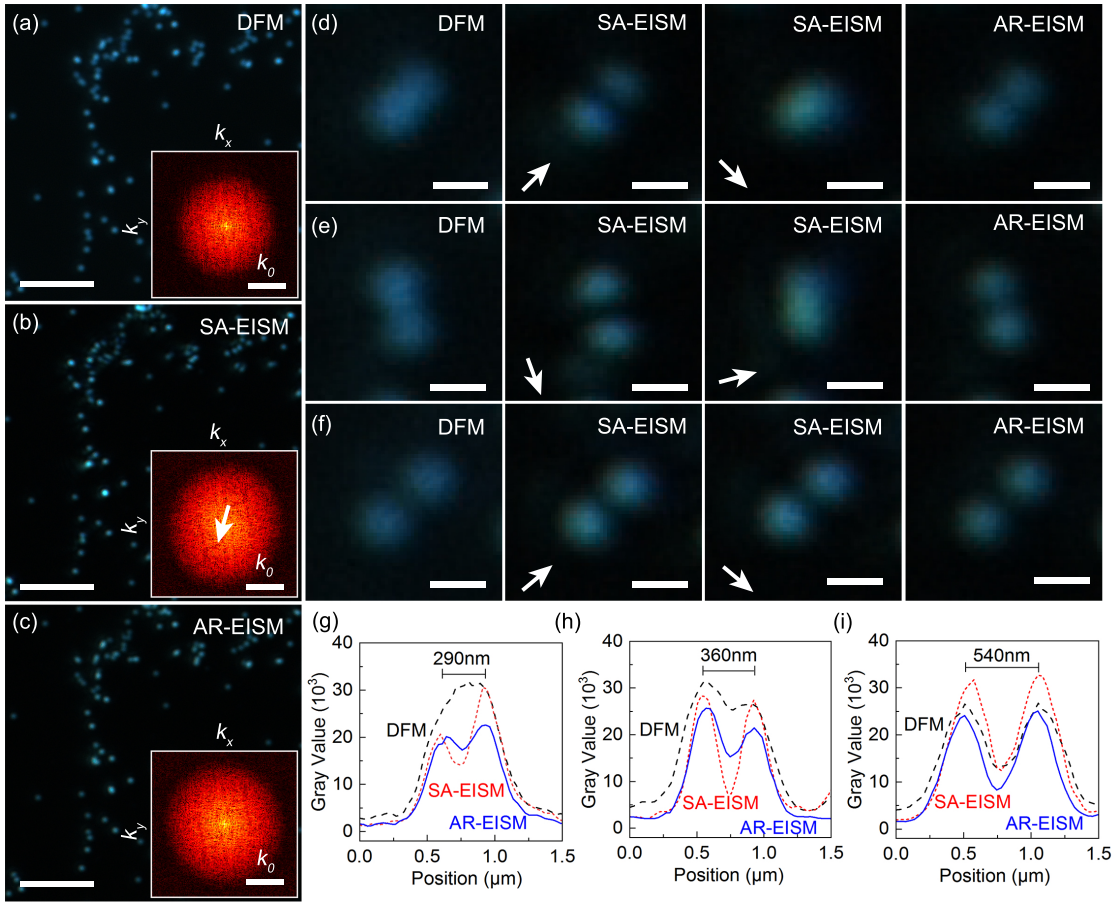


Fig. 3. Imaging of 150-nm-diameter PS particles. (a) DFM; (b) SA-EISM; (c) AR-EISM images. The center-to-center separations in (d)–(f) are 290 nm, 360 nm, and 540 nm, respectively. The arrows indicate the EW propagation direction. Panels (g)–(i) correspond to (d)–(f), respectively. The SA-EISM intensity profiles are measured with the EW propagation direction parallel to the line connecting the particle centers. Exposure time: 1 s. Scale bars: 5 μm in (a)–(c) and 0.5 μm in (d)–(f).

those obtained with AR-EISM were 0.134, 0.264, and 0.528, respectively. PS particle pairs with different center-to-center separations and orientations can be resolved in a single acquisition, whereas SA-EISM requires adjustment of the illumination direction to identify a suitable azimuthal orientation. Therefore, SA-EISM is advantageous for samples with predominantly unidirectional features that demand high resolution along a specific direction, whereas AR-EISM is better suited for samples containing structures of varying orientations. It delivers more uniform resolution across all azimuthal directions, albeit at the cost of lower resolution than SA-EISM achieves under its optimal illumination condition. In addition, quantitative analysis demonstrates that AR-EISM achieves higher SNR and imaging contrast.

The images were further analyzed using a point spread function (PSF) model to quantitatively evaluate the spatial resolution. The PSF characterizes the response of an optical system to a point-like object, where a narrower PSF generally indicates higher spatial resolution. Here, 100-nm-diameter PS particles were used as point-like objects to characterize the PSFs of the two imaging systems. The corresponding images acquired with DFM and AR-EISM are shown in Figs. 4(a) and 4(b), respectively. The full widths at half maximum (FWHMs) of the PSFs for DFM and AR-EISM are 393 nm and 294 nm, respectively (Fig. 4(e)). Based on statistical analysis of approximately 20 particles, the distributions of the PSF widths for DFM and AR-EISM were fitted to normal distributions, yielding mean values of approximately 385 nm and 293 nm, respectively (Fig. 4(e)). For AR-EISM, the measured mean PSF width of approximately 293 nm is close to the theoretical Abbe diffraction limit of 283 nm. Furthermore, two 150-nm-diameter PS nanoparticles with a center-to-center separation of 290 nm (corresponding to an edge-to-edge gap of 140 nm) were marginally resolved.

Although the DFM image exhibits higher overall intensity, the contours of the 20-nm-diameter TiO_2 nanowires are less distinct, particularly in regions where multiple nanowires overlap or intersect (Fig. 4(f)). In contrast, AR-EISM provides a more uniform intensity distribution and enhanced contrast between the nanowires and background, enabling individual nanowires to be more readily distinguished, even in partially overlapping regions (Fig. 4(g)). In DFM, regions with densely stacked nanowires exhibit locally saturated signals, whereas isolated nanowires appear relatively weak and have reduced contrast. These intensity variations are substantially suppressed in AR-EISM, resulting in more uniform and distinguishable features for both stacked and isolated nanowires. The intensity profiles shown in Fig. 4(j) further confirm the enhanced contrast and improved feature separation achieved by AR-EISM compared with DFM.

DFM uses oblique illumination to direct unscattered light away from the imaging path, allowing scattered light to

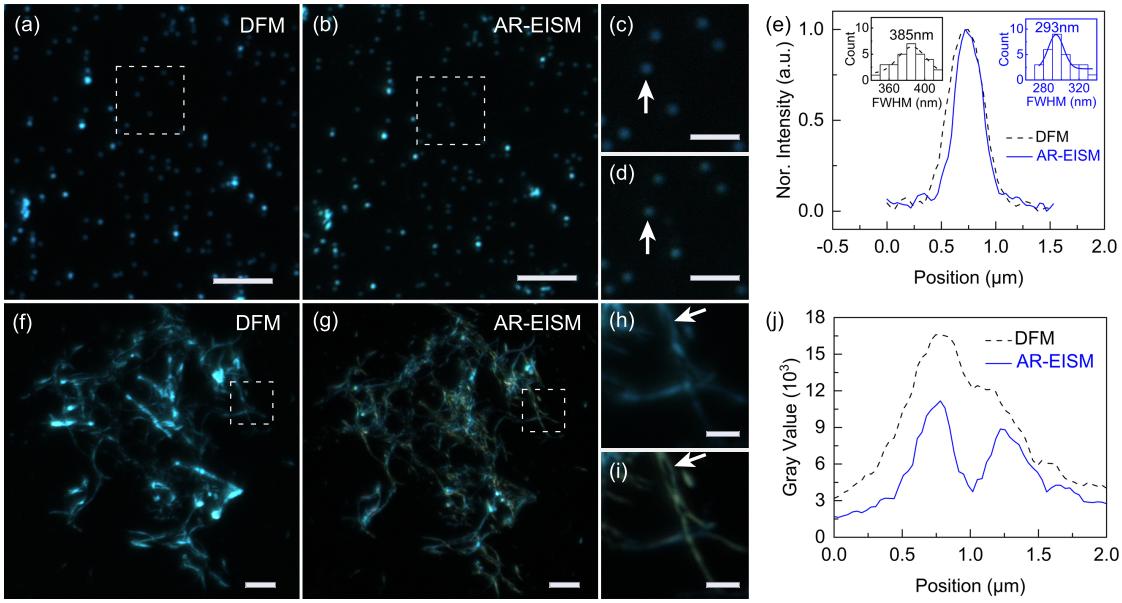


Fig. 4. Imaging of 100-nm-diameter PS particles and 20-nm-diameter TiO_2 nanowires. (a), (f) DFM images; (b), (g) AR-EISM images. (c), (d) and (h), (i) show magnified views of the boxed regions in (a), (b) and (f), (g), respectively. (e) shows the intensity profile of the arrow-indicated PS particle, with the statistical distribution of the PSF width shown in the inset. (j) shows the intensity profile of the TiO_2 nanowire. Exposure time: 1 s. Scale bars: 5 μm in (a), (b), (f), and (g), and 2 μm in (c), (d), (h), and (i).

dominate the image and yielding strong signals and well-defined contours. In contrast, the improved performance of AR-EISM is primarily attributed to the surface-selective nature of EW illumination rather than EW-induced SFS, since the limited collimation of incoherent illumination prevents the formation of a well-defined single-mode evanescent field. Accordingly, the frequency-shifting effect is not expected to dominate the imaging process, consistent with the measured resolution remaining close to the diffraction limit rather than exhibiting pronounced super-resolution. The exponential decay of the evanescent field confines illumination to the vicinity of the interface, suppressing background scattering and out-of-focus stray light. The resulting improvement in the effective signal-to-noise ratio and image contrast facilitates the discrimination of closely spaced nanoscale structures, whereas azimuthal integration reduces the directional dependence of spatial resolution and improves imaging uniformity. Nevertheless, the mechanical scanning mechanism in the current AR-EISM system limits its capability for dynamic imaging. High-speed beam-steering strategies, including galvanometric scanning, SLM-based beam rotation, and electro-optic steering, could replace mechanical rotation, potentially enabling AR-EISM to be used for dynamic imaging.

In conclusion, AR-EISM was developed for high-contrast, label-free imaging. While single-azimuth EISM provides enhanced lateral resolution, its performance depends on the evanescent-wave propagation direction. By continuously rotating the illumination azimuth over 360° during a single exposure, AR-EISM reduces this directional dependence via multiazimuthal integration. Imaging of PS particles yielded a 1.37-fold increase in SNR and higher contrast relative to conventional DFM. Quantitative PSF analysis returned a mean PSF width of 293 nm for AR-EISM, close to the theoretical Abbe diffraction limit of 283 nm. Furthermore, AR-EISM marginally resolved particle pairs with a center-to-center separation of 290 nm, corresponding to a 140 nm edge-to-edge gap. Imaging of TiO_2 nanowires further confirmed the improved contrast and feature separation achieved by AR-EISM over DFM.

Funding. National Natural Science Foundation of China (62505138); Natural Science Foundation of the Jiangsu Higher Education Institutions of China (25KJB510012).

Disclosures. The authors declare no conflicts of interest.

Data availability. Data underlying the results presented in this paper are not publicly available at this time but may be obtained from the authors upon reasonable request.

REFERENCES

1. P. F. Gao, G. Lei, and C. Z. Huang, Anal. Chem. **93**, 4707 (2021).
2. G. Vishnyakov, G. Levin, V. Minaev, *et al.*, Opt. Lett. **41**, 3037 (2016).
3. T. L. Nguyen, S. Pradeep, R. L. Judson-Torres, *et al.*, ACS Nano **16**, 11516 (2022).
4. J. Ortega Arroyo, D. Cole, and P. Kukura, Nat. Protoc. **11**, 617 (2016).
5. M. Küppers, D. Albrecht, A. D. Kashkanova, *et al.*, Nat. Commun. **14**, 1962 (2023).
6. R. Diekmann, Ø. I. Helle, C. I. Øie, *et al.*, Nat. Photonics **11**, 322 (2017).
7. S. B. Dutta, W. Hübner, P. Goffing, *et al.*, Sci. Adv. **12**, eaeg3960 (2026).
8. P. Zhang, L. Zhou, R. Wang, *et al.*, Nat. Commun. **13**, 2298 (2022).
9. D. J. Hill, C. W. Pinion, J. D. Christesen, *et al.*, ACS Photonics **1**, 725 (2014).
10. N. Jayakumar, L. E. Villegas-Hernández, W. Zhao, *et al.*, Light. Sci. Appl. **14**, 259 (2025).
11. X. Yang, H. Zhang, Y. Zhang, *et al.*, Commun. Eng. (2026).
12. P. von Olshausen and A. Rohrbach, Opt. Lett. **38**, 4066 (2013).
13. F. Jünger, P. v Olshausen, and A. Rohrbach, Sci. Rep. **6**, 30393 (2016).
14. F. Jünger, D. Ruh, D. Strobel, *et al.*, Nat. Commun. **13**, 1758 (2022).
15. C. Pang, X. Liu, Q. Zhang, *et al.*, Adv. Photonics Res. **5**, 2300341 (2024).